PERGAMON

Carbon 40 (2002) 375–382

CARBON

Evolution of BET internal surface area in glassy carbon powder during thermal oxidation

A. Braun[a,b,*], M. Bärtsch[a], B. Schnyder[a], R. Kötz[a], O. Haas[a], A. Wokaun[a,b]

[a]*Paul Scherrer Institute, General Energy Research Department, CH-5232 Villigen PSI, Switzerland*
[b]*Department of Chemical Engineering and Industrial Chemistry, Swiss Federal Institute of Technology, ETH-Zentrum, CH-8092 Zürich, Switzerland*

Received 1 February 2001; accepted 18 April 2001

Abstract

It is demonstrated that glassy carbon powder can be thermochemically activated. During activation, a film with open pores is created on the glassy carbon particles. This film has a large internal surface area, which is accessible to liquids and gases. A simple model for the evolution of the internal surface area in glassy carbon powder during thermochemical gas-phase oxidation is also presented and compared with experimental data. Experimental results are in qualitative agreement with the model. We found that a sharp particle size distribution is desirable with regard to potential technical applications. © 2002 Elsevier Science Ltd. All rights reserved.

Keywords: A. Glass-like carbon; B. Activation; C. BET surface area, Modeling; D. Surface areas

1. Introduction

Glassy carbon (GC) is a material having voids of about 1 to 2 nm diameter, which are closed and separated from each other. Due to its pore volume, GC has a mass density of about 1.5 g/cm^3, which is rather low compared to graphite, which has a density of 2.26 g/cm^3 [1–3]. It has been reported that the pores can be opened and enlarged by thermochemical gas-phase oxidation [4,5]. Such activated GC can be utilized as a material for electrochemical double layer capacitors [6–8]. The activation creates a film with open pores on the surface of the GC, which envelopes the non-activated and therefore impermeable interior material [4]. We found that film growth is a chemical process controlled by diffusion of reactants and products in the film [4]. The film growth is superimposed by a second process, which burns off the film due to combustion. This process was found to be controlled by the chemical reaction of carbon with oxygen. In previous works we studied the thermochemical oxidation of GC sheets and disks with thicknesses between 60 and 1000 microns extensively [4,5,9]. We extended our investigations to GC powder, which consists of GC spheres with a diameter smaller than 15 microns. Unlike monolithic GC samples with an outer film and an internal non-activated core, which is a prerequisite for a bipolar cell-assembly [6,7], the powder GC should consist of only activated material [10] and then be processed to form a regular powder electrode, including graphite and binder. The polydispersity of the powder has the disadvantage that the smaller particles vanish during the activation due to combustion, while the larger particles still consist of an outer shell of active film and an inner core, which is not yet activated. We activated GC powder similar to the sheet samples and measured the BET internal surface area as a function of the activation time. Section 2 describes the material studied and the activation process applied. A simple geometrical model is established in Section 3, which describes the evolution of the specific internal surface area of GC spheres during activation. In Section 4, experimental data for the burn-off and for the BET surface area are presented. Experimental data were fitted to the model and

*Corresponding author. Lawrence Berkeley National Laboratory, Environmental Energy Technology Division, One Cyclotron Road, MS 70-108 B, Berkeley, CA 94720, USA. Tel.: +1-510-486-7257; fax: +1-510-486-7303.

E-mail address: abraun@lbl.gov (A. Braun).

0008-6223/02/$ – see front matter © 2002 Elsevier Science Ltd. All rights reserved.
PII: S0008-6223(01)00114-2

checked for consistency with results reported for monolithic samples. Different results for different GC materials are discussed in terms of their different microstructure, as studied with X-ray diffraction.

2. Experimental

2.1. Description of the GC material

Commercially available glassy carbon powder was purchased: SIGRADUR K and SIGRADUR G. The two types of GC are abbreviated K and G below. K (G) was obtained from pyrolysis of a phenolic resin at a temperature of about 1000°C (2200°C). The particle volume fraction X vs. particle radii as displayed in Fig. 1 was certificated by the manufacturer. The particles were declared to have a sphere-like shape and diameter between 0.4 and 12 microns (G: 1–4 microns), which was confirmed in our laboratory with an optical microscope. The G spheres are mostly smaller than the K spheres. The maximum of the volume distribution is at 4 μm for G and at 12 μm for K. The average values for the radii were calculated as follows:

$$\langle R \rangle = \frac{\int_0^\infty P(R) \cdot R \, \mathrm{d}R}{\int_0^\infty P(R) \, \mathrm{d}R} \tag{1}$$

where $P(R)$ is the particle radii distribution as displayed in Fig. 2. For the K-type powder (G) a value of 5.50 microns (2.05) was found.

For a specific evaluation of the data it is necessary to know the volume fraction, as displayed in Fig. 1, and also the distribution of the particle size, i.e. the particle radii fraction Y_i, as shown in Fig. 2. The conversion from

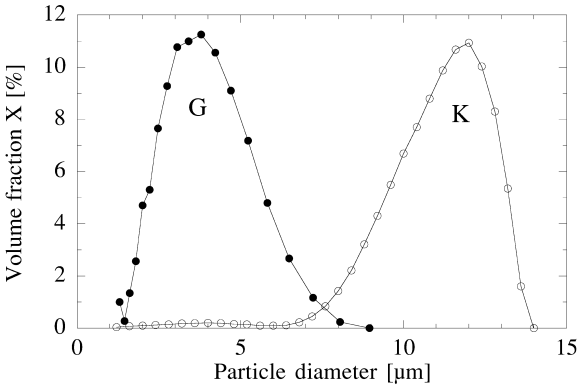

Fig. 1. Distribution of volume fraction X_i of GC powder SIGRADUR K (open symbols) and G (closed symbols).

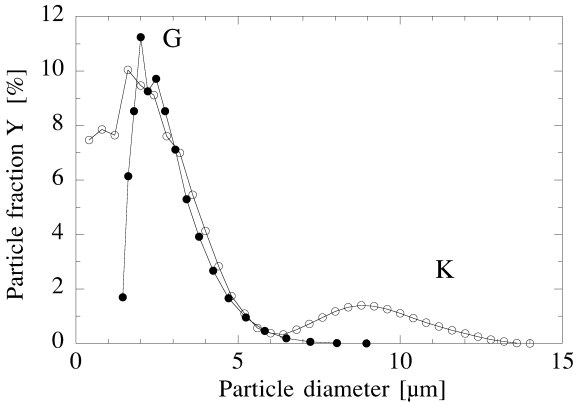

Fig. 2. Distribution of the particle diameter Y_i of GC powder SIGRADUR K (open symbols) and G (closed symbols).

volume distribution X to particle distribution Y is obtained from

$$X_i = \frac{V_i}{V} = \frac{N_i \cdot (4/3)\pi R_i^3}{V} \tag{2}$$

where V is the volume of all the N particles in a specific amount of powder, N_i of them having radius R_i, and V_i is therefore is the fraction of the volume arising from particles with radius R_i. Thus, $V = \Sigma_i V_i$ and

$$Y_i = \frac{N_i}{N} = \frac{V}{N} \frac{X_i}{(4/3)\pi R_i^3}. \tag{3}$$

Only the quantities X_i and R_i are needed in the conversion to obtain the distribution $P(R)$. The results of the conversion are displayed in Fig. 2.

For the mass density of non-oxidised GC, the values reported by the manufacturer were used (K, $\rho_i = 1.53$ g/cm^3; G, $\rho_i = 1.49$ g/cm^3). These values are in line with data reported in the literature [1].

Mass densities for the active GC film were not available with the exception of K-type GC sheets of 60 microns thickness: $\rho_i \approx 1.2$ g/cm^3 [11].

The internal surface area (BET) of the activated GC per active film volume was assumed to be 900 m^2/g for the K powder (G: 200 m^2/g), because the measured data tend to this value for long activation times. Additionally, from investigations of K-type 1 mm GC disks and 60 micron GC sheets we know that their active films have a BET surface area of around 900 m^2/g for long activation times [4,5,11].

2.2. Oxidation of GC

GC powder was thermally oxidised in the following manner. The powder was suspended in ethanol and then poured into a ceramic dish of 12 cm diameter. The dish was shaken by hand in order to cover the dish walls with a

thin film of the GC–ethanol suspension. Within a few seconds, the ethanol evaporated and a thin film of GC powder was left behind on the ceramic dish. The area covered by the powder was typically about 100 to 150 cm^2. Care was taken to minimize agglomeration of the GC in order to ensure that as many free particles as possible were spread over the dish surface, so that every powder particle had contact with the air or oxygen. The dish was then placed in a preheated furnace at 450°C. After a specified time, the dish with the oxidised GC was removed from the furnace. A whole set of powder samples activated at 450°C but for different times was prepared in the same way. The quantity of activated GC powder was typically about 150 to 300 mg. The relative weight loss $m(t)/m_0$ of the K-type powder was determined with a high-precision laboratory microbalance. Gas adsorption measurements were carried out with N_2 on a Micromeritics ASAP 2000 test station. The BET surface area of the powder (m^2/g) was determined from isothermal plots.

3. Establishing the model

From investigations on GC sheets and disks we know that a film with open porosity can be grown on the surface of GC [4,5,9,11]. These samples have a sandwich-like structure with an unactivated core with closed pores, which is enveloped by the film with open pores. We found that the thickness of the active film on flat samples follows a growth law which can essentially be represented by a so-called *Generalized LambertW function* $\mathcal{G}$, which can be approximated by a square-root function [9]. Such square-root-type growth behaviour is a typical indication of a diffusion-controlled growth process. Film growth in samples of spherical shape cannot be described accurately by $\mathcal{G}$. An approximation would be to consider the film growth in non-shrinking spheres; the solution of this problem is also exact and can be found in Ref. [12]. Since we found, however, that this somewhat difficult solution does not differ significantly from a simple square-root function, which is actually applied to non-shrinking flat samples, we decided to choose this function as an approximation.

The thickness of an arbitrarily shaped object decreases linearly with reaction time when the burn-off is constant and homogeneous. Therefore, the radii of the spheres decrease linearly with activation time, as demonstrated in Ref. [12] and as found experimentally for flat GC samples [4,5,9,11].

The evolution of the internal surface area arising from open pores, which are created only by oxidation, can be monitored by gas adsorption measurements.

The oxidation of a spherical GC particle can be divided into several stages, as illustrated in Fig. 3:

1. Initially, there is a non-activated GC sphere with radius R_0 and mass density ρ_i.
2. Upon oxidation, an outer shell with radius $r_e(t)$ of active film material with mass density ρ_e is created, and the active volume envelopes a non-activated core with radius $r_i(t)$, which contributes to the weight of the powder, but not to the internal surface area. The thickness of the shell is

$$\Theta(t) = r_e(t) - r_i(t) \geq 0. \tag{4}$$

   The film growth represents a diffusion-controlled process, which is characterized by the film growth rate γ, with dimensions $m/s^{1/2}$ for flat samples [12].
3. Burn-off of the outer sphere occurs, and $r_e(t)$ decreases linearly:

$$r_e(t) = R_0 - \beta t \geq 0 \tag{5}$$

   where β is the burn-off constant. The inner radius r_i shrinks according to the relation

$$r_i = R_0 - \beta t - \Theta(t) \geq 0 \tag{6}$$

   and the function $\Theta(t)$ is the expression for the film thickness.
4. After a specific time there is no longer an unactivated GC core, but only active film material.

Note that steps (2) and (3) take place at the same time. However, during the initial stage of the reaction the film growth is more pronounced than the burn-off. From this point, only the fully activated GC sphere with radius $r_i(t)$ is burning off. We assume that the ratio

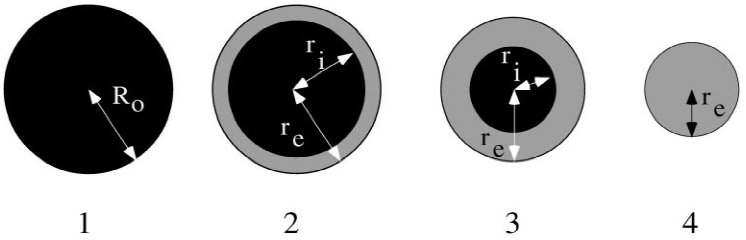

Fig. 3. Illustration of changes in pore radii during oxidation. Unreacted core shrinking and shrinking particle size during the reaction (grey film and black core).

$$\Omega = \frac{\text{Internal surface area of the film}}{\text{Mass of the film}} \tag{7}$$

remains constant during activation. From studies of GC plates, however, we know that this ratio can decrease to about two-thirds of its initial value during 2 h of activation at 450°C, because pores grow and coalesce during activation at the cost of the internal surface area [4,5,9,11]. Since the amount of activated material decreases, the total internal surface area also decreases. The ratio Ω may differ, however, if different types of GC are considered. For K (G)-type GC powder, Ω is about 900 (200) m^2/g.

The radii $r_e(t)$ and $r_i(t)$ change upon oxidation and are therefore time dependent. For the growth of an active film, it is necessary that the active film growth rate exceeds the burn-off rate. The internal surface area of an arbitrary amount of powder as a function of the activation time can be calculated within this model.

The mass of a partially activated sphere consists of the mass of the unreacted core of mass density ρ_i and radius $r_i(t)$:

$$m_i(t) = \rho_i \tfrac{4}{3}\pi r_i^3(t) \tag{8}$$

plus the mass of the surrounding film of mass density ρ_e and film thickness $\Theta(t) = r_e(t) - r_i(t)$:

$$m_e(t) = \rho_e \tfrac{4}{3}\pi(r_e^3(t) - r_i^3(t)). \tag{9}$$

The total surface area S of a particle which can be covered by an adsorbent gas consists of its geometrical surface area

$$S_{\text{geom.}}(t) = 4\pi r_e^2(t) \tag{10}$$

and the internal surface area of the active film volume

$$S_{\text{int.}}(t) = \tfrac{4}{3}\pi\Omega\rho_e(r_e^3(t) - r_i^3(t)) \tag{11}$$

where Ω is the internal surface area of the active mass (m^2/g) as in Eq. (7). The contribution of the geometrical area to the overall surface area is only minor when particles with an active film are considered.

The total surface area S per mass m is

$$S^*_{(t)} = \frac{S_{\text{geom.}} + S_{\text{int.}}}{m_i + m_e} = \frac{3r_e(t)^2 + \Omega\rho_e(r_e(t)^3 - r_i(t)^3)}{r_i(t)^3(\rho_i - \rho_e) + r_e(t)^3 \cdot \rho_e}. \tag{12}$$

The function $S^*(t)$ is piecewise defined because the radii r_e and r_i vanish at specific times t_e and t_i, which are defined implicitly by the relations

$$r_e(t_e) = R_0 - \beta t_e = 0 \text{ and } r_i(t_i) = R_0 - \beta t_i - \Theta(t_i).$$

Eq. (12) represents the internal surface area of a sphere during oxidation.

For a somewhat more accurate evaluation and comparison with experimental data, the distribution of the radii R_0, the mass densities and the time dependence of the radii and the maximum achievable BET surface area per gram must be known and taken into account.

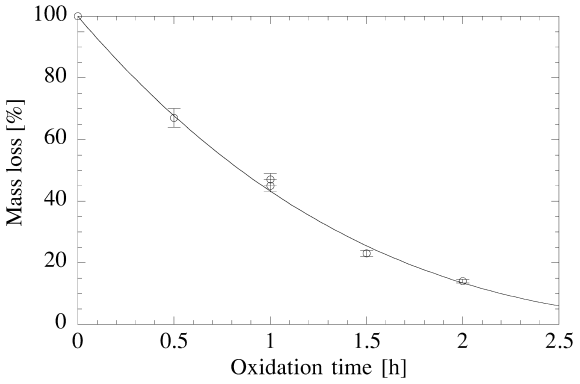

Fig. 4. Relative burn-off (%) of K powder at 450°C activation temperature. The line represents the least-square fit according to Eq. (16).

The size distribution of the spheres, however, changes during oxidation. In particular, the distribution is shifted towards smaller radii, and the larger particles dominate the distribution on account of the smaller particles, which vanish during oxidation due to combustion. This complicates the computation of the surface area of polydisperse powders considerably and is beyond the scope of this work. Computation will therefore be restricted to a monodisperse distribution in this work.

4. Results and discussion

4.1. Burn-off

The relative mass loss of the K powder during oxidation is displayed in Fig. 4. The burn-off rates of GC powder as determined by the mass loss are listed in Table 1. In previous experiments with GC plates we found that the burn-off rates were constant [4]. For comparison, they are also listed in Table 1.

Since the radius of the particle decreases linearly during oxidation, we can derive a third power time dependency of the weight loss during oxidation:

Table 1
Experimentally obtained burn-off rates β and active film growth rates γ for various GC sheets (K) of different thickness and GC powder

Temp. (°C)	Thickness (μm)	Growth γ (μm/$\sqrt{h}$)	Burn-off β (μm/h)
450	1000	38.7	22
450	60	11.0	3.7
450	K powder (≈12 μm)	–	2.2±0.6
450	G powder (≈5 μm)	–	0.83±0.3

$$r_e = R_0 - \beta t \tag{13}$$

$$V_e(t) = \tfrac{4}{3}\pi r_e^3(t) = \tfrac{4}{3}\pi(R_0 - \beta t)^3 \tag{14}$$

$$V_e(t) = \frac{m(t)}{\rho_i} = \frac{4}{3}\pi R_0^3\left(1 - \frac{\beta t}{R_0}\right)^3 \tag{15}$$

$$m(t) = m_0\left(1 - \frac{\beta t}{R_0}\right)^3. \tag{16}$$

In this derivation we have neglected the fact that a minor part of the weight loss arises from the evolution of the active film, which is manifested by a decrease of the mass density from about 1.5 to about 1.2 g/cm^3. An expression of the type

$$m(t) = m_0 \cdot \left(1 - \frac{\beta \cdot t}{R_0}\right)^3 \tag{17}$$

was fitted to the experimental mass loss data for the K-type GC powder (Fig. 4). A radius of $R_0 = 6.8$ μm for the K powder spheres and a burn-off rate of 1.6 μm/h were obtained. Since the particle size distribution is not taken into account in this expression, the data obtained by this fitting procedure can only serve as a rough approximation. The K powder particle radius, however, is in good agreement with the particle size distribution as specified by the manufacturer (Figs. 1 and 2). We recall that the mean particle radius $\langle R \rangle$ for K, obtained from the manufacturer's reported particle size distribution, was 5.5 microns.

We found that, after about 150 min oxidation, K powder was no longer visible in the furnace, provided it had been well spread over the Petri dish surface before oxidation. This indicates that the largest K powder particles, which have a diameter of around 14 microns, vanish after this time.

The burn-off rate β for the K powder obtained in this way was 7 μm/150 min = 2.8 μm/h. Since mass loss due to active film growth was not taken into account, β is overestimated. The value 2.8 μm/h therefore represents an upper limit for β. The burn-off rate of 60 microns K-type GC sheet as mentioned above was found to be about 3.7 μm/h at the same activation temperature. Similar considerations and observations for the G powder yield a burn-off rate of around 0.83±0.3 microns/h.

We found that the K powder has a larger burn-off rate than the G powder. This result was expected. G-type glassy carbon is pyrolyzed at a much higher temperature than K-type glassy carbon. G-type GC therefore has larger crystallites and fewer defects and impurities than K-type GC. G has crystallites with larger basal planes and few edge planes. Oxidation and thus burn-off occur more readily at the edges of the crystallites, while the basal planes are quite resistant to reaction. Consequently, the G powder has a smaller burn-off rate than the K powder.

Table 1 also contains the burn-off rates of monolithic GC sheets of different thicknesses. Samples of 1000 micron thickness have a burn-off rate a factor of 6 larger than the 60 micron samples, although these samples received the same pyrolysis treatment. We believe that pyrolysis gases evolving during pyrolysis disturb crystal growth in GC, and for thick samples the release of pyrolysis gases lasts longer than for thin samples. Therefore, the disorder in the 1000 micron samples is more pronounced than in the 60 micron samples, provided they have experienced identical pyrolysis schedules. The thin 60 micron K-type GC sheets have a burn-off rate somewhat larger than that of the K powder. The burn-off rate increases with sample thickness.

Unlike the mass loss due to burn-off of the sheet and disk GC samples, which was found to be linear, the weight loss of the powder in the dishes was found to decrease at the third power of the sphere radius, which is expected for spherical particles [12].

In this model we assume for the GC powder: (i) as a rough approximation a rate γ of active film growth which is proportional to a square-root-like function of oxidation time; and (ii) a constant rate β for the burn-off of GC material with

$$r_e(t) = R_0 - \beta t \geq 0, \quad r_i(t) = R_0 - \beta t - \gamma t^{1/2} \geq 0.$$

Note that the growth rates and burn-off rates in Table 1 deviate considerably for different types of GC.

4.2. BET surface area

Figs. 5 and 6 display the evolution of the specific internal surface area of both types of GC powder during activation. The total internal surface area shows a convex increase with increasing activation time. Before activation, only the outer geometrical area contributes to the BET surface area, because the non-activated GC has no porosity which can be accessed by the nitrogen from outside. This

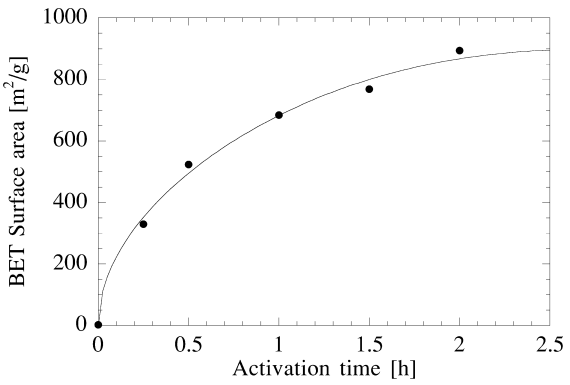

Fig. 5. Measured and calculated (———, Eq. (12)) BET surface areas of Sigradur K. Parameters: $\beta = 1.26$ μm/h; $\gamma = 4.76$ μm/$\sqrt{h}$; $\Omega = 900$ m^2/g; $R_0 = 6$ μm; $\rho_i = 1.53$ g/cm^3; $\rho_e = 1.2$ g/cm^3.

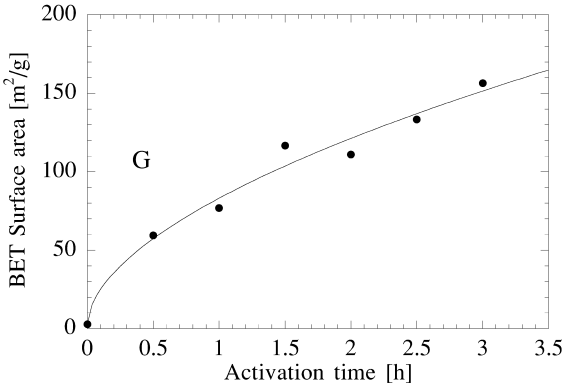

Fig. 6. Measured and calculated (———, Eq. (12)) BET surface areas of Sigradur G. Parameters: $\beta = 0.36$ μm/h; $\gamma = 1.0$ μm/$\sqrt{h}$; $\Omega = 200$ m^2/g; $R_0 = 2.5$ μm; $\rho_i = 1.49$ g/cm^3; $\rho_e = 1.2$ g/cm^3.

contribution is very small prior to activation. With activation, however, a porous film builds up. Since the film thickness increases, the overall internal surface area also increases.

For the K powder, an increase of the internal surface area from about 2 m^2/g with no activation to about 900 m^2/g after 2 h of activation is observed (see Fig. 5). A larger value for longer activation times is not expected, because the powder is consumed after about 120 to 150 min of activation. The specific surface area of 900 m^2/g is in line with results reported for activated GC sheets [4,11].

For G-type GC powder, an increase of the internal surface area from about 2 m^2/g before activation to about 200 m^2/g after 3 h of activation is observed (see Fig. 6).

Previous electrochemical measurements on thermochemically activated GC sheets, both K-type and G-type, showed that the electrochemical double layer capacitance is by far lower for G-type GC than for K-type GC [11]. The electrochemical double layer capacity matches the results from the BET measurements.

For the non-activated GC powder, no direct information on its internal, closed surface area was available. There should not be major differences in the internal surface areas of K (G) powder and monolithic K (G) sheets, because their microstructures do not differ significantly from each other (see subsection X-ray diffraction for further discussion). We therefore assume that the micropore sizes and internal surface areas are similar for monolithic samples and powders. Possibly the G powder has fewer and larger pores than the K powder, since G sheets have fewer and larger pores than K sheets.

4.3. Fitting

Fig. 5 displays the measured BET surface area of the K powder and a least-squares fit computed according to Eq. (12) with sphere radius $R_0 = 6$ microns (12 μm diameter). Note that Eq. (12) is only applicable to a monodisperse distribution of the powder spheres. The best fit is obtained with a radius of 6 μm, a burn-off rate of 1.26 μm/h, and a film growth rate of 4.76 μm/$\sqrt{h}$. For the densities, $\rho_i = 1.53$ g/cm^3 and $\rho_e = 1.2$ g/cm^3 were taken. The radius of 6 μm semi-quantitatively matches the maximum of the particle size distribution (6 μm, see maximum of the distribution in Fig. 1).

The particle number distribution in Fig. 2 shows that a very large proportion of the particles is smaller than 4 microns. The particles smaller than 4 microns are burnt off within 1 h and no longer contribute to the BET surface area for activation times exceeding 1 h. From the technological point of view this means that some of the material is wasted, unless powder with a sharper particle size distribution is utilized.

The burn-off rate obtained by fitting the BET surface area evolution data to Eq. (8) (1.26 μm/h) is smaller by a factor of 2 than the experimentally determined burn-off rate determined by the weight loss experiment. The film growth rate obtained by fitting is 4.76 μm/$\sqrt{h}$. No experimental film thickness data for powder particles were available for comparison. In the investigation of the monolithic samples, film thicknesses were obtained directly from microscopic images of fracture cross sections of the activated plates and sheets, but this technique was not applicable to powders. However, from Table 1 a trend can be derived such that thick GC samples have a larger film growth rate than thin GC samples. In our studies on GC plates with different thicknesses we found that the film growth and burn-off rates depend on the thickness of the plates, and this could be systematically attributed to differences in their structure [9,11]. The powder spheres are the thinnest samples due to their small radius and therefore have a smaller film growth rate, when the trend is obeyed.

Fig. 6 displays the measured BET surface area of the G powder as well as a least-squares fit to Eq. (12). With a particle diameter of 5 microns and $\rho_i = 1.49$ g/cm^3, the burn-off rate was found to be 0.36 μm/h and differs by roughly a factor of 2 from the value obtained experimentally (0.83 μm/h). The film growth rate was found to be 1.0 μm/$\sqrt{h}$. This value is lower than the corresponding value for the K powder (4.76 μm/$\sqrt{h}$), as expected [11]. The results are summarized in Table 2.

Table 2
Burn-off rates β and active film growth rates γ of GC powder, as obtained from the least-squares fit of Eq. (12) to BET data

Type of GC	Diameter (μm)	Growth γ (μm/$\sqrt{h}$)	Burn-off β (μm/h)
K powder	12	4.76	1.26
G powder	5	1.0	0.36

The deviations in the burn-off rates by a factor of about 2 for both powders in Tables 1 and 2 can be explained by the fact that the fitting routine applies Eq. (12), which is based on the assumption that all powder spheres are freely distributed, whereas the real experiment could not fully guarantee that all powder spheres were free. Also, it was assumed that the internal surface area of the powder, Ω, is constant during oxidation.

4.4. X-ray diffraction

Fig. 7 displays X-ray diffractograms of the two different kinds of non-activated GC powders studied. Only the (002) peak at about 25° is shown, the only well-developed peak of glassy carbon. The curve with the lower intensity is from the K powder; the curve with the higher intensity is from the G powder. By Bragg's law, the position of this peak is correlated with the distance of parallel graphene layers. By the Scherrer formula, the full width at half maximum of this peak is related to the crystallite size. Since the 2Θ value of the intensity maximum of the K powder diffractogram is shifted somewhat to the left from that of the G powder, the average distance of the graphene sheets in K powder is larger than in G powder.

The large difference in intensity reveals that the G powder has a higher stage of crystallinity than the K powder. The full width at half maximum (FWHM) of the (002) peak for the G powder is qualitatively smaller than that of the K powder. This reveals that the G powder consists of carbon with larger crystallites, while the K powder contains smaller crystallites. Similar results have been reported for sheet and disk samples of K-type and G-type glassy carbon [11].

Fig. 8 displays the diffractograms of the corresponding GC plates with 1 mm thickness. The G-type sample has an overall larger diffracted intensity than the K-type GC, a smaller FWHM of the (002) peak, and the position of the

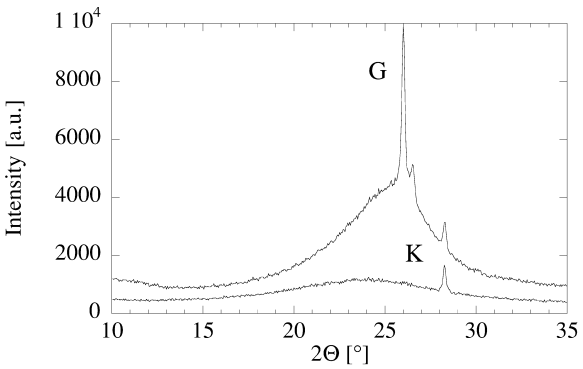

Fig. 7. X-ray diffractograms of GC powders K (lower curve) and G (upper curve). Peaks around 28° are from corundum in the grain mill. The peak around 26° in the diffractogram for G could originate from highly crystalline graphite particles.

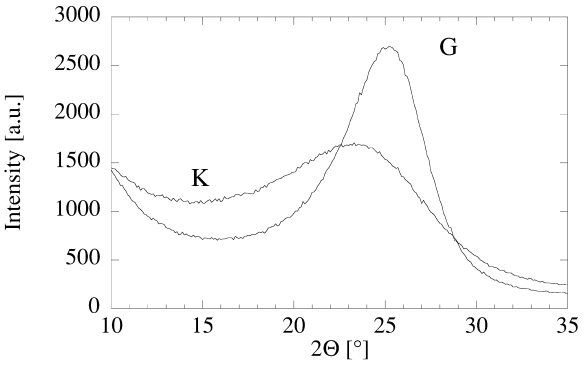

Fig. 8. X-ray diffractograms of K and G GC plates of 1 mm thickness.

(002) peak is at a smaller 2Θ value than that of the K-type GC. The diffractograms reveal that structural differences in the G-type GC powder and K-type GC powder are similar to the structural differences in the monolithic plates. G-type GC therefore has larger crystallites and fewer defects than K-type GC. This observation is valid both for the powder and for monolithic samples. It is probably the higher stage of crystallinity (larger crystallites, fewer defects, graphene layer distance closer to that of graphite) which enables the G-type glassy carbon to better resist burn-off. This result is in line with the findings for burn-off, because the K plates burn off in a shorter time (or at lower temperature) than the G plates. Also, the K powder burns off faster (in a shorter time at the same temperature) than the G powder.

G-type GC has larger pores than K-type GC, as is generally known from small-angle X-ray scattering (SAXS) experiments [1]. Since it is not the pore space, but the pore walls, that accounts for the internal surface area, it is evident that the K powder with the smaller pores, but roughly the same porosity as the G powder, has a larger internal surface area. We measured K and G GC sheets with SAXS and found that the pores in G-type GC are twice as large in diameter as those in K-type GC [13]. Assuming that the pores are sphere-like, then the area S_p of a single pore with radius R_p is given by

$$S_p = 4\pi R_p^2 \tag{18}$$

and the area of a sphere with a radius twice as large is

$$S_p^* = 4\pi(2 \cdot R_p)^2 = 4 \cdot S_p. \tag{19}$$

Therefore, the internal surface area of G-type GC is smaller than for K-type GC, provided the number of pores per unit volume remains unchanged during pyrolysis. The four times larger internal surface area of activated K-type (900 m^2/g) vs. G-type (200 m^2/g), as measured here, reflects these considerations well.

5. Conclusions

We have demonstrated that glassy carbon (GC) powder can be thermochemically activated in the same way as plate-like GC samples, as found by BET adsorption measurements. The active film is grown on top of the surface and envelopes a non-activated core. This core contributes to the overall powder sample weight, but not to the internal surface area. We adopted the previously published model for film growth on shrinking flat samples and extended it in order to model the evolution of the internal surface area of GC powder. The model implies that the specific internal surface area of the powder follows a square-root-like trend as a function of oxidation time. Such a trend was found experimentally for the two different types of GC studied in this work.

The expression for the total surface area could be fitted to the experimental data with surprising accuracy, despite several simplifications made in the quantitative treatment of the system (assumed monodisperse particle size distribution; constant specific surface area; square-root-like growth law on particles with spherical symmetry). Fit results such as particle radius, film growth rate and burn-off rate were consistent with experimentally observed data or with data from other studies. Differences in internal surface area and burn-off of GC for different pyrolysis temperatures (K and G) could be explained by their different microstructures. We expect a better agreement between experimental and calculated results when (i) experimental data for the film growth rates of the powders and (ii) a more precise expression for the film growth, similar to that found for flat samples, are available.

For technical applications it is desirable to have a powder with a very sharp particle size distribution in order to minimize the loss of activated material due to burn-off.

Acknowledgements

This research was supported financially by the Board of the Swiss Federal Institute of Technology within the Swiss Priority Program on Materials Research. Collaborations with ABB Corporate Research, Baden (Switzerland), and Leclanché S.A., Yverdon Les Bains (Switzerland), are gratefully acknowledged. We are grateful to F. Geiger, who carried out the adsorption measurements.

References

[1] Jenkins GM, Kawamura K. Polymeric carbons — carbon fibre, glass and char, 1st ed., Cambridge, UK: Cambridge University Press, 1976.
[2] Lewis JC, Redfern B, Cowlard FC. Solid-State Electron 1963;6:251.
[3] Cowlard FC, Lewis JC. J Mater Sci 1967;2:507.
[4] Braun A, Bärtsch M, Schnyder B, Kötz R, Haas O, Goerigk G et al. X-ray scattering and adsorption studies of thermally oxidised glassy carbon. J Non-Cryst Solids 1999;260:1–14.
[5] Braun A, Bärtsch M, Geiger F, Schnyder B, Kötz R, Haas O et al. A study on oxidised glassy carbon carbon sheets for bipolar supercapacitor electrodes. In: Doughty DH, Nazar LF, Arakawa M, Brack H-P, Naoi K, editors. New materials for batteries and fuel cells. Mater Res Soc Symp Proc 2000;575:369–381.
[6] Bärtsch M, Braun A, Kötz R, Haas O. High-power electrochemical double-layer capacitor. In: Proceedings of the 38th Power Sources Conference, Cherry Hill, NJ, 1998, pp. 17–21.
[7] Bärtsch M, Braun A, Schnyder B, Kötz R, Haas O. Bipolar glassy carbon electrochemical double-layer capacitor: 100,000 cycles demonstrated. J New Mater Electrochem Syst 1999;2:273–7.
[8] Miklos J, Mund K, Naschwitz W. Siemens AG, Offenlegungsschrift DE 30 11 701 A1, Deutsches Patentamt, 1980.
[9] Braun A, Bärtsch M, Schnyder B, Kötz R. A model for the film growth in samples with two moving boundaries — an application and extension of the unreacted-core model. Chem Eng Sci 2000;55(22):5273–82.
[10] Schüler C, Kötz R. Mehrschichtige Elektrode für elektrochemische Anwendungen. Application No. 98/134, Swiss Intellectual Property Office, 1998.
[11] Braun A. Development and characterization of glassy carbon electrodes for a bipolar electrochemical double layer capacitor. Dr. sc. nat thesis, ETH Zürich, 1999.
[12] Levenspiel O. Chemical reaction engineering, Wiley, 1972.
[13] Braun A, Bärtsch M, Schnyder B, Kötz R, Haas O. Investigation of the porous structure of glassy carbon by SAXS — an application of synchrotron radiation. PSI Scientific Report 1998, vol. V. Villigen, Switzerland: Paul Scherrer Institut, 1999;34–35 (ISSN 1423-7342).